Modelling of vibrocompaction using hypoplasticity with intergranular strains

Modélisation du vibrocompactage en utilisant l'hypoplasticité et les déformations intergranulaires

M. Arnold & I. Herle
Institute of Geotechnical Engineering, TU Dresden, Germany

ABSTRACT

Soils can be best compacted by repeated shearing. The strain amplitude plays an important role for the maximum compaction that can be reached. Experimental evidence emphasises a vital impact of simultaneous multidirectional shear loading on the rate and magnitude of soil compaction.

Vibrocompaction by deep vibration was studied in the light of these findings by numerical simulations. In a dynamic FE analysis with elastic material behaviour strain paths were determined. Since shear stiffness strongly degrades with increasing magnitude of shear strain, a strain amplitude-dependent stiffness was introduced. The FE calculations were run multiple times to iterate the appropriate secant stiffness for each distance from the vibrator. Subsequently, the strain paths were used to control element simulations using again the intergranular strain enhanced hypoplastic constitutive model.

RÉSUMÉ

Les sols sont d'autant mieux compactés qu'on leur applique un cisaillement répété. L'amplitude de la déformation joue un rôle important dans la compacité qui peut être atteinte. Les résultats expérimentaux ont démontrés la grande efficacité des charges de cisaillement multidirectionelles simultanées sur le taux de compacité du sol.

A la lumière de ces éléments, le vibrocompactage par vibration profonde a été étudié grâce à des simulations numériques. Une analyse dynamique aux éléments finis d'un matériau élastique a ainsi permis de déterminer les chemins de déformation. Comme le module de cisaillement baisse fortement avec l'augmentation des déformations de cisaillement, un module de cisaillement dépendant de l'amplitude des déformations de cisaillement a été introduit dans la modélisation. Les calculs ont été menés par itérations successives afin d'adapter les valeurs des modules sécants des terrains en fonction de la distance du compacteur. Enfin, les chemins de déformations ont été utilisés pour contrôler les simulations en utilisant à nouveau le modèle de sol amélioré basé sur l'hypoplasticité et les déformations intergranulaires.

Keywords : vibrocompaction, small strain stiffness, hypoplasticity, intergranular strains

1 INTRODUCTION

The mechanical behaviour of granular soils is markedly influenced by their density. Loose soils are softer and can mobilize less shear resistance than dense soils. Loose soils are usually less uniform and tend to liquefaction. Consequently, there is a demand for the densification of loose granular soils for construction purposes.

This paper presents results of numerical computations of the vibrocompaction method using horizontally circling deep vibrators. First, a dynamical 3-D simulation of elastic medium within a disc-shaped domain produced a loading sequence for several selected points around the vibrator. Subsequently, the obtained strain paths were used for a control of numerical element tests with an advanced constitutive model.

The compaction of soil is equivalent with a reduction of the volume of voids, the latter being usually described by void ratio. Hence, constitutive models applied for the simulation of compaction processes should, besides other requirements, incorporate void ratio or an analogous parameter.

Hypoplastic models include void ratio as a state variable and, thus, they well meet the above mentioned condition. In order to simulate cyclic stress and strain paths in coarse grained soils, a version of the hypoplastic model by von Wolffersdorff (1996) with the intergranular strain enhancements of Niemunis & Herle (1997) can be used.

2 CALCULATION PROCEDURE

A dynamic FE calculation using a 3D geometry together with a hypoplastic model with intergranular strains would be a suitable method to simulate vibrocompaction. However, there are at least two drawbacks with this approach: Firstly, there is little experience using this constitutive model in dynamic calculations, yet. Secondly, the computational effort is enormous.

Therefore, a calculation procedure analogue to Kessler et al. (2006) was chosen. In the first step, a dynamic Finite Element analysis was performed in order to obtain strain paths. The FE code Tochnog (2006) was used for the elastic analysis of a 3D disc-shaped model wave propagation analyses. The solution was carried out in the time domain. In the second step, the obtained strain paths were used as an input for hypoplastic element calculations simulating the densification during the cyclic vibrator loading.

3 CONSTITUTIVE MODELLING

The soil was modelled by the hypoplasticity with intergranular strains (Niemunis & Herle 1997, von Wolffersdorff 1996) using the parameter set of Keßler et al. (2006).

The initial density of the soil was assumed to be very low. An initial void ratio e_0 of 0.85 was chosen. A dry density of

doi:10.3233/978-1-60750-031-5-2334

1.43 g/cm³ was obtained with an assumed particle density of 2.65 g/cm³ (quartz sand).

Like shown by Niemunis & Herle (1997), the constitutive model is able to reproduce a realistic degradation of shear stiffness with strain. Using the chosen constitutive constants, numerical biaxial tests were conducted to simulate the stiffness degradation for different states of the strain history. The initial void ratio was set to 0.85 and the isotropic initial stress state to $\sigma_{11} = \sigma_{22} = \sigma_{33} = -0.14$ MPa. This corresponds to an average stress at the modelled depth of 15 m. Different strain histories were introduced by an appropriate initialization of the state variable intergranular strain.

Fig. 1 shows the secant modulus $G_{sec} = (\sigma_{11} - \sigma_{22})/(\varepsilon_{11} - \varepsilon_{22})$ plotted versus shear strain $\Delta\gamma = |\varepsilon_{11} - \varepsilon_{22}|$. Hardin & Drnevich (1972) presented a widespread equation of the stiffness degradation with strain. Recently, a modified approach was suggested by Hardin & Kalinski (2005):

$$G_{sec}(\Delta\gamma) = \frac{G_{sec}}{1 + \frac{\Delta\gamma}{\gamma_r}\left[1 + a \cdot \exp\left(-b\frac{\Delta\gamma}{\gamma_r}\right)\right]} \quad (1)$$

Eq. 1 was used to fit the curve of a strain reversal (180° curve) of Fig. 1 via the parameters $G_{sec,0}$, γ_r and a. The parameter b was set to 1 like proposed by Hardin & Kalinski (2005). The best fit yielded parameter $a < -1$ resulting in an initial increase of the shear modulus with strain. Because of this contradiction to the observed behaviour, a was set to -1 to ensure a monotonic decrease of the shear stiffness with strain. $G_{sec,0} = 110$ MPa and $\gamma_r = 2.2 \cdot 10^{-3}$ were obtained from this fit.

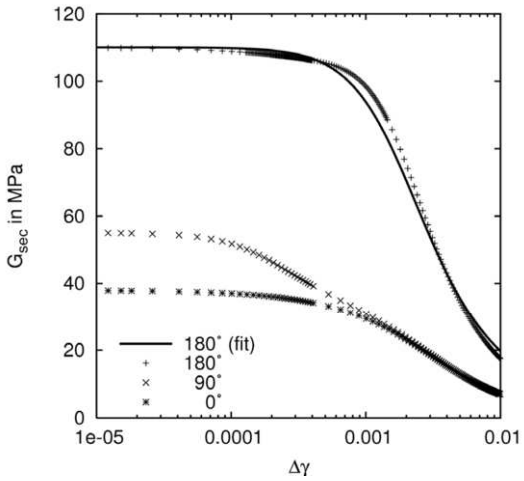

Figure 1. Calculated secant stiffness for a biaxial compression with constant volume after a change of strain path direction.

The fit of Eq. 1 was used to create a link between the hypoplasticity and elasticity with variable stiffness. Provided that there is a cyclic shear strain loading $\gamma(t) = \gamma_A \cdot \cos(\varpi \cdot t)$ (Fig. 2a), the shear strain direction reverses at $t = 0$. $\Delta\gamma$ in Eq. 1 increases from zero at $t = 0$ to $2\gamma_A$ at $t = \pi/\varpi$. Hence, the shear stiffness starts at $G_{sec,0}$ and decreases with strain to a value of $G_{sec}(2\gamma_A)$ at $t = \pi/\varpi$ (Fig. 2b). At this time, the direction reverses again. $\Delta\gamma$ starts from zero and the shear stiffness degradation starts once again from $G_{sec,0}$.

Based on the relationship between G_{sec} and $\Delta\gamma$, it is possible to assign to each material point, which is oscillating with a shear strain amplitude γ_A, a corresponding shear modulus G_{sec}. Since the shear strain amplitude is not known a priori, it has to be iteratively approached by multiple runs of the elastic FE calculation. The shear modulus G_{sec}^{i} of the run i follows from γ_A^{i-1} of the previous run (i-1). The Poisson's ratio of 0.28 was kept constant.

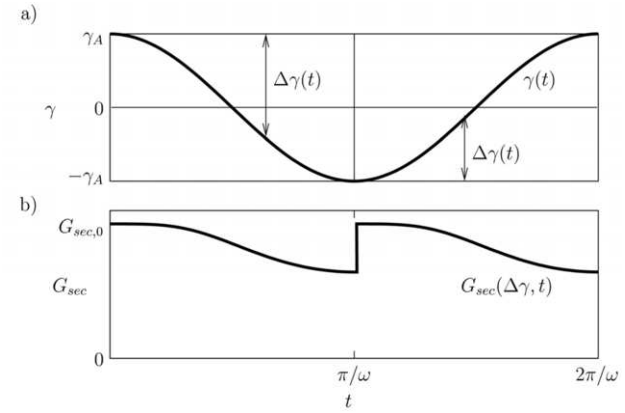

Figure 2. a) Shear strain vs. time, b) secant shear modulus vs. time during one strain cycle.

4 FE MODEL OF DYNAMIC ANALYSIS

A 3D disc-shaped model was used. It has an exterior radius of 15 m and a height of 0.5 m. It represents a soil layer which is located at a depth between 14.5 and 15 m below the ground surface. The soil volume is discretized by 4-node tetrahedral elements. The irregular mesh consisting of more than 12,000 elements is shown in Fig. 3. The maximum length of an element side is 0.7 m. This is approx. 1/3 of the ocurring smallest wave length and therefore sufficient to capture the propagation of the waves.

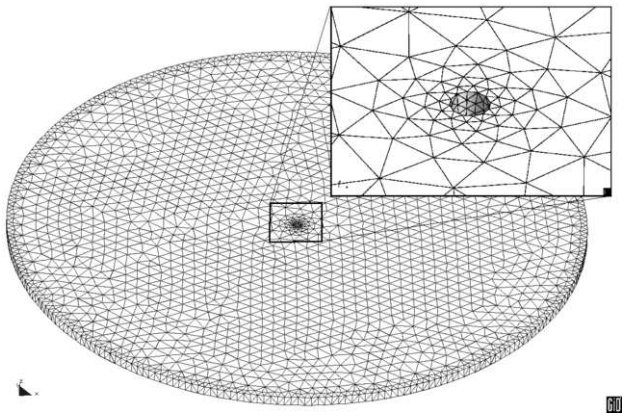

Figure 3. FE mesh.

The vibrator has a radius of 0.2 m and a length of 3.0 m. It was not discretized. Instead, a cylindric hole in the disc at the position of the vibrator was considered (see zoom in Fig. 3).

Due to the geometry of the model it is convenient to use a cylindrical coordinate system. The disc spreads in the plane described by the polar coordinates r and θ. The symmetry axis of the disc coincides with the axis z.

A viscous boundary (Lysmer & Kuhlmeyer 1969) was applied at the circumference to minimize reflections of impinging waves, since in reality the wave would run to infinity. Based on the shear modulus $G_{sec,0}$ and using the parameters $a = 1$ and $b = 0.25$ in the approaches of Lysmer & Kuhlmeyer (1969) yield a viscous damping of 710 kNs/m³ for the pressure wave and 98 kNs/m³ for the shear wave. For the sake of stress equivalence to the real 3D situation, the disc was perpendicularly loaded at the top and at the bottom with an average vertical stress in this depth, even though this does not influence the calculated strains in the elastic model.

The movement of the vibrator results from the complex interaction of vibrator and soil and is influenced by numerous parameters. The movement of the vibrator was simulated by velocity boundary conditions of the same amplitude at the

surface nodes of the cylindric hole. This assumption represents a strong simplification.

The deep vibrator was assumed to be hinged at its top (2.5 m above the disc surface). Thus, the surface nodes were moved along a circular path with a radius of 7.5 mm at the bottom and of 6.25 mm at the top of the disc. The applied frequency was 30 Hz.

Several calculation steps were needed in order to get a consistent distribution of the strain-dependent stiffness within the discretized domain. Each step consisted of 30 cycles. In the initial step, a constant Young's modulus following from the initial shear modulus $G_{sec,0}$ was assumed (cf. Section 3).

The strain paths with all six components of the strain tensor were registered in 20 points along the radial direction of the model. After approximately 10 cycles the transient effects vanished and the oscillation amplitudes of all six strain components became steady and could be generalized. A scalar shear strain amplitude γ_A was obtained from the maximum second invariant of the strain tensor. The resulting stiffness could be calculated at the selected eight points using Eq. 1.

In the next step, a strain-dependent stiffness was distributed along the radial direction using a multi-linear function. Six additional steps were performed in this way. A fast convergence was observed within the iteration process.

5 RESULTS OF DYNAMIC ANALYSIS

At time t = 1 s the initial equilibrium iteration is finished. The calculation starts with three dynamic cycles with the amplitude increasing linearily from zero to the 7.5 mm. The aim of this procedure is to minimize transient effects. 27 dynamic cycles with a total duration of three seconds follow. The response of a point at a radius of 2.8 m located in a depth of 14.75 m was chosen as an example.

Figures 4 (a) and (b) show the evolution of strains. A similar transient effect is observed as for the velocities. Normal strains ε_{rr} and $\varepsilon_{\theta\theta}$ exhibit the largest magnitudes, the shear strain components $\varepsilon_{\theta z}$ and ε_{rz} are very small.

In Fig. 4 (c) two cycles are zoomed out of Fig. 4 (b). The figure manifests the dominating excitation frequency with its sinus shape as well as the phase shifts, which occur due to differing wave velocities for different wave types.

It has been shown that the excitation frequency dominates the strains. Thus, it is meaningful to consider only this frequency. To approximate the strain path, the equation

$$\varepsilon_{\alpha\beta} = a_{\alpha\beta} \sin\left(2\pi \frac{t}{T} + b_{\alpha\beta}\right) \tag{2}$$

was assumed for each strain component $\varepsilon_{\alpha\beta}$ with $\alpha,\beta \in \{r,\theta,z\}$. The period T of a cycle was 1/30 s. For each strain component Eq. 2 was fitted to the calculated data via $a_{\alpha\beta}$ and $b_{\alpha\beta}$ in the time domain (1.5 s < t ≤ 2.0 s).

The strain amplitudes obtained from the approximation (Eq. 2) are plotted for different radii in Fig. 5. Since the amplitudes differ by the order of magnitude, a logarithmic scale is used. The largest amplitudes of most strain components occur near the vibrator. With increasing distance from the vibrator the amplitudes decrease. This general pattern results predominantly from the geometrical damping. This effect is further emphasized by the strain-dependent stiffness, which is low close to the vibrator and becomes high in the outer domains of the considered disc volume.

6 HYPOPLASTIC ELEMENT SIMULATIONS

It is assumed that a soil particle in the compacted continuum oscillates in the horizontal directions r and θ around a fixed position. Hence, all strains regarding the horizontal position of the particle form closed loops. In the vertical direction the soil particle oscillates, too, but it also moves downward due to the densification of the grain skeleton. Consequently, the vertical strain ε_{zz} does not follow a closed loop. However, the geostatic vertical stress σ_{zz} is known and can be applied as a boundary condition in the vertical direction.

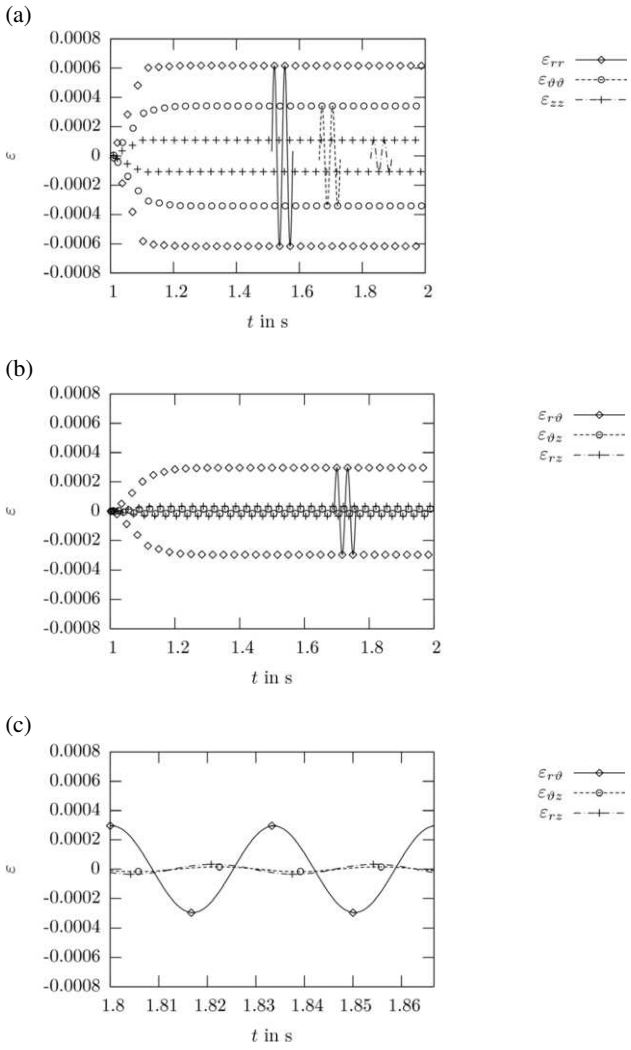

Figure 4 (a) Envelope of maximum normal strains, (b) envelope of maximum shear strains and (c) shear strains of two selected cycles at a distance 2.8 m from the symmetry line in the deep vibrator problem.

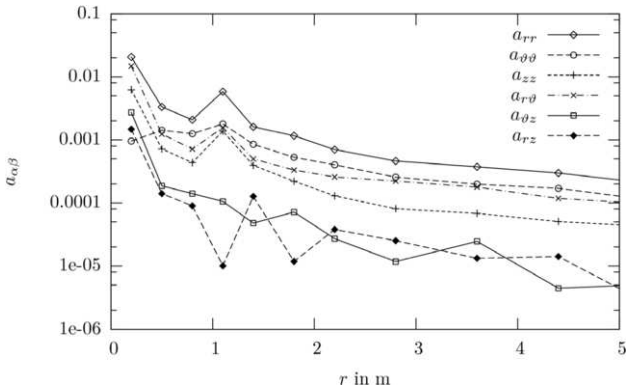

Figure 5. Magnitude of strain amplitudes (logarithmic). Elastic analysis.

This idealization was used in the hypoplastic simulations with the element test program HYPTEST (Herle 1997). The strain paths obtained in the elastic FE analyses were applied as a test control. Since the hypoplastic model is formulated in rates, the strain rates were prescribed using the time derivative of Eq. 2.

The initial void ratio of the loose soil was set to 0.85. The initial stress state was considered as $\sigma_{rr} = \sigma_{\theta\theta} = 0.1$ MPa and $\sigma_{zz} = 0.2$ MPa. For each of the eight selected points, 120 cycles have been calculated.

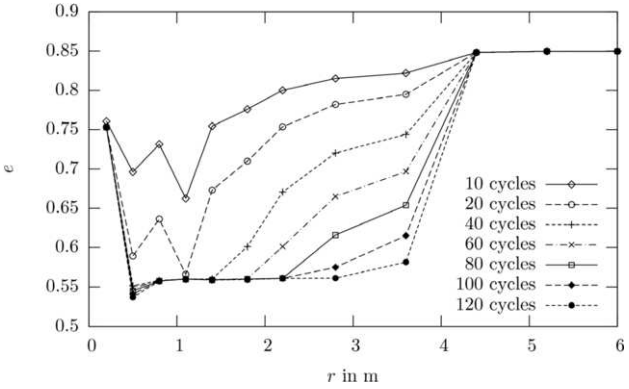

Figure 6. Evolution of void ratio along radial distance from the vibrator.

The evolution of void ratio with strain cycles can be seen in Fig. 6. Starting from the initial value of 0.85, void ratio reduces with progressing cycles. The rate of the reduction decreases with time. Thus, the first 20 cycles lead to a larger change in void ratio than the second 20 cycles, and so on.

Three zones may be distinguished. In the first zone close to the vibrator ($r < 0.5$ m), the densification fades out after only a few cycles without reaching the minimum void ratio. This effect, which has been observed also in the field application of vibrocompaction, is caused by large strain amplitudes in this domain. At the beginning of a shear deformation process, soil behaves contractant. But if shear strains grow further on, the soil becomes dilatant. Hence, contractancy and dilatancy balance each other and an overall volumetric deformation vanishes.

In the second zone within approximately $0.5 \text{ m} < r < 3.0 \ldots 4.0$ m the compaction process succeeds to approach a pressure dependent minimum void ratio. Contractancy prevails and the soil reaches a densification limit. In this zone vibrocompaction works at best. The larger the distance from the vibrator, the slower the compaction progress.

Only 60 cycles suffice to reach the densest state, while in the field application several thousand cycles are required. The model seems to predict a too fast compaction rate, probably due to the simplifying assumptions in the model formulation. E. g., the influence of pore water was disregarded. Since compaction is based on the reduction of pore volume, water has to flow out of the densified soil. Due to a final permeability even of coarse grained soils this would take certainly more time than two seconds. Probable liquefaction phenomena make the situation even more complex. Furthermore, the elastic approach does not cover the damping caused by shocks (Fellin 2000).

The third zone is characterized by a constant void ratio and spreads behind the second zone. There, strain amplitudes are too small to surpass the reversible elastic strain range. This zone is not affected by the vibrocompaction.

7 CONCLUSIONS

This paper presents an advanced numerical analysis of vibrocompaction. Using hypoplasticity with intergranular strains enables the modelling of the compaction process. For the dynamic wave propagation analyses, an advanced elastic approach was used, which includes the dependence of stiffness on the shear strain.

The obtained compaction profiles show three zones known from the field evidence: A moderate compaction close to the vibrator, a zone of maximum compaction and a zone without any compaction effect away from the vibrator.

In spite of the demanding computations within the presented analysis, several important effects were not considered:

- The influence of pore water and thus a potential liquefaction of soil due to the undrained response during the short time of vibration.
- A realistic interface between the vibrator and soil which can take into account slip effects after reaching the maximum shear stress at the contact.
- A general 3-D model which does not require an assumption of constant stresses at the boundaries of the disc-shaped domain.

Due to the omitted effects mentioned above as well as due to several simplifications that have been made, there are discrepancies between the obtained results and experience in situ, especially regarding the evolution of densification in time. Further research should clarify the particular role of the above stated items.

AKNOWLEDGEMENT

This work was supported by Keller Holding GmbH, which is gratefully acknowledged.

REFERENCES

Fellin, W. 2000. Rütteldruckverdichtung als plastodynamisches Problem. In *Advances in Geotechnical Engineering and Tunneling*, Vol.2, Balkema, Rotterdam.

Hardin, B. O. & Drnevich, V. P. 1972. Shear modulus and damping of soils: Design equations and curves. *ASCE Journal of the Soil Mechanics and Foundations Division*, Vol. 98, No. 7, 667-692.

Hardin, B. O. & Kalinski, M. E. 2005. Estimating the shear modulus of gravelly soils. *ASCE Journal of Geotechnical and Geoenvironmental Engineering,* Vol. 131, No. 7, pp. 867-875.

Herle, I. 1997. *Hypoplastizität und Granulometrie einfacher Korngerüste*. Dissertation. Heft 142, Veröffentlichungen des Institutes für Bodenmechanik und Felsmechanik der Universität Fridericiana in Karlsruhe.

Herle, I. & Gudehus, G. 1999. Determination of parameters of a hypoplastic constitutive model from properties of grain assemblies. *Mechanics of Cohesive-Frictional Materials,* Vol. 4, No. 5, pp. 461-486.

Keßler, S., Heibrock, G. & Triantafyllidis, T. 2006. On prediction of vibrocompaction performance using numerical models. In *Symposium International TRANSVIB 2006*, Gonin, Holeymann, Rocher-Lacoste, (eds). Editions du LCPC, Paris, pp. 233-242.

Lysmer, J. & Kuhlemeyer, R. L. 1969. Finite dynamic model for infinite media. *ASCE Journal of Engineering Mechanics Division,* Vol. 95, No. EM4, pp. 859-877.

Niemunis A. & Herle I. 1997. Hypoplastic model for cohesionless soils with elastic strain range. *Mechanics of Cohesive-Frictional Materials,* Vol. 2, No. 4, pp. 279-299.

Tochnog 2006, Tochnog Professional Version 4.1. http://www.feat.nl.

von Wolffersdorff, P. A. 1996. A hypoplastic relation for granular materials with a predefined limit state surface.*Mechanics of Cohesive-Frictional Materials,* Vol. 1, No. 4, pp. 251-271.

Wichtmann, T., Niemunis, A. & Triantafyllidis, T. 2005. Strain accumulation in sand due to cyclic loading: drained triaxial tests. *Soil Dynamics and Earthquake Engineering,* Vol. 25, No. 12, pp. 967-979.